Supplement of Atmos. Chem. Phys., 21, 8377–8392, 2021
https://doi.org/10.5194/acp-21-8377-2021-supplement

Atmospheric Chemistry and Physics
Open Access
EGU

Supplement of

New methodology shows short atmospheric lifetimes of oxidized sulfur and nitrogen due to dry deposition

Katherine Hayden et al.

Correspondence to: Shao-Meng Li (shaomeng.li@pku.edu.cn) and Katherine Hayden (katherine.hayden@canada.ca)

The Supporting Information contains the following sections:

Section 1. Supporting Tables S1 to S3.

Table S1. Instrumentation and measurement details for SO_2, NO_y and pSO_4.

Measurement	Instrument	Sampling time resolution (s)	Detection limit	Manufacturer
SO_2	Thermo 43iTLE	1	0.7 ppbv	Thermo Fisher Scientific, Franklin, MA, USA
NO_y	Thermo 42iTL	1	0.09 ppbv	Thermo Fisher Scientific, Franklin, MA, USA
pSO_4	Aerosol Mass Spectrometer	10	0.048 ug m^{-3}	Aerodyne Research Inc.

Table S2. Measurement and model-derived estimates of cumulative deposition (%), transport distance (km) and lifetimes (hrs) of TOS and TON for F7, F19 and F20. Geographic foot print areas under the plumes for TOS and TON are also provided.

	Cumulative deposition (%)				**e-folding transport distance ($d_{1/e}$) (km)**				**Lifetime ($\tau = d_{1/e}/u$) (hrs)**			
TOS	7	19	20		7	19	20		7	19	20	
Measurements	22±4	74±5	45±3		1230±290	71±1	210±4		26	2.2	6.5	
Model	7	21	8		4300	500	2800		large	16	91	
Footprint (km^2)	3500	5700	4200									
TON	7	19	20 (SP)	20 (NP)	7	19	20 (SP)	20 (NP)	7	19	20	
Measurements	31±11	49±11	62±14	34±6	360±14	190±7	62±1	290±30	7.6	5.6	1.9	9.0
Model	3	19	4	2	4300	650	2000	2400	91	23	63	78
Footprint (km^2)	3500	5700	4200	3100								

Table S3. Equivalent dry deposition velocities V_d (cm s^{-1}) determined from the aircraft measurements (AC) and the model. SO_2 and TON mixing ratios were taken from the average of the lowest ~40m (interpolated values) across the plume width for two sets of screens. SP=south plume, NP=north plume for F20.

Flight	**SO_2**		**TON**	
	AC	**model**	**AC**	**model**
7	0.9±0.6	0.76	2.3±0.7	1.32
	1.5±0.3	0.67	3.2±1.0	1.55
mean	***1.2±0.5***	***0.72***	***2.8±0.8***	***1.44***
19	2.3±0.5	0.52	1.9±0.6	1.10
	2.8±0.5	0.67	1.3±0.4	1.35
	2.3±0.4	0.70	1.5±0.5	1.40
mean	***2.4±0.4***	***0.63***	***1.6±0.5***	***1.28***
20	3.5±0.6	0.63	6.7±2.0 (SP) 4.2±1.3 (NP)	1.06 (SP) 0.94 (NP)
	3.2±0.5	0.52	2.8±0.8 (SP) 0.18±0.05 (NP)	0.77 (SP) 0.85 (NP)
mean	***3.4±0.6***	***0.58***	***4.7±0.1.4 (SP)*** ***2.2±0.7 (NP)***	***0.92 (SP)*** ***0.90 (NP)***

Table S4. Prescribed values used in the Monte-Carlo simulations with five different deposition algorithms.

Component	Input Range	Units	Algorithm	Reference
Friction velocity (U*)	0.2 to 0.6	unitless	All 5 algorithms	Oski-ôtin ground site observations
Obukhov Length (L)	-200 to -350	m	All 5 algorithms	Oski-ôtin ground site observations
Reference Height (Z)	40 to 45	m	All 5 algorithms	Estimate of AOSR
Roughness Length (z0)	0.6 to 1	unitless	All 5 algorithms	Grassi et al., 2013
Schmidt Number (S_c)	0.8 to 2	unitless	All 5 algorithms	Oski-ôtin ground site observations
Leaf Area Index (LAI)	2 to 5	unitless	All 5 algorithms	Makar et al., 2018; Brook et al., 1999
Minimum Leaf stomatal resistance for H_2O (rs_{min})	100 to 250	s/m	ZHANG, C5DRY, WESLEY, GEM_MACH	Zhang et al., 2003
Canopy Height (h_c)	6 to 18	m	C5DRY	Estimate of AOSR
Ground resistance (R_g)	100 to 250	s/m	All 5 algorithms	Wesley et al., 1989
Solar Radiation (SolarRG)	450	W/m^2	ZHANG, C5DRY, WESLEY, GEM-MACH	Oski Otin ground site observations
Mesophyll resistance (R_m)	0.03 to 0.05	s/m	ZHANG, C5DRY, NOAH-GEM	Makar et al., 2018
In canopy aerodynamic	20 to 60	s/m	ZHANG, WESLEY, GEM-	Zhang et al., 2003

resistance reference (R_{ac0})			MACH, NOAH-GEM	
Cuticle resistance (R_{cut})	500 to 1000	s/m	C5DRY	Based on calculations of R_{cut} from the other deposition algorithms
Dry cuticle reference ($R_{cut,d0}$)	2000	s/m	ZHANG, WESLEY, NOAH-GEM	Zhang et al., 2002
Dry cuticle reference (R_{cuti})	1000	s/m	GEM-MACH	Makar et al., 2018
Surface Temperature (T_s)	20 to 25	°C	ZHANG, C5DRY, WESLEY, GEM-MACH	Aircraft observations
Relative Humidity (RH)	55 to 70	%	ZHANG, C5DRY, GEM-MACH, NOAH-GEM	Aircraft observations
Solar Zenith Angle (Theta)	65 to 75	unitless	ZHANG, C5DRY	https://www.esrl.noaa.gov/gmd/grad/antuv/SolarCalc.jsp
Slope gas exchange data (m)	9 to 10	unitless	NOAH-GEM	Zhang et al., 2002
Intercept gas exchange data (b)	0.01 to 0.04	unitless	NOAH-GEM	Zhang et al., 2002
Net CO_2 assimilation rate (A_n)	$1e^{-6}$ to $4e^{-6}$	mol $C/m^2/s$	NOAH-GEM	Baldocchi et al., 1997
RH fraction at the leaf surface (h_s)	0.5 to 1	unitless	NOAH-GEM	Estimated range

Atmospheric pressure (P)	101300	Pa	NOAH-GEM	Aircraft observations
CO_2 partial pressure at the leaf surface (C_s)	23 to 37	Pa	NOAH-GEM	Niyogi et al., 2009
Ambient T at height Z (T_a)	20 to 25	°C	ZHANG, C5DRY, GEM-MACH	Aircraft observations
T_{min}	-5 to 0	°C	ZHANG, C5DRY, GEM-MACH	Makar et al., 2018
T_{max}	40 to 45	°C	ZHANG, C5DRY, GEM-MACH	Makar et al., 2018
T_{opt}	15 to 30	°C	ZHANG, C5DRY, GEM-MACH	Makar et al., 2018
Molecular diffusivity of SO_2 (D_c)	0.1085	cm^2/s	All 5 algorithms	Massman et al., 1998
Molecular diffusivity of water (D_{H2O})	0.2178	cm^2/s	All 5 algorithms	Massman et al., 1998

40

41

Section S2. Supporting Figures S1 to S5.

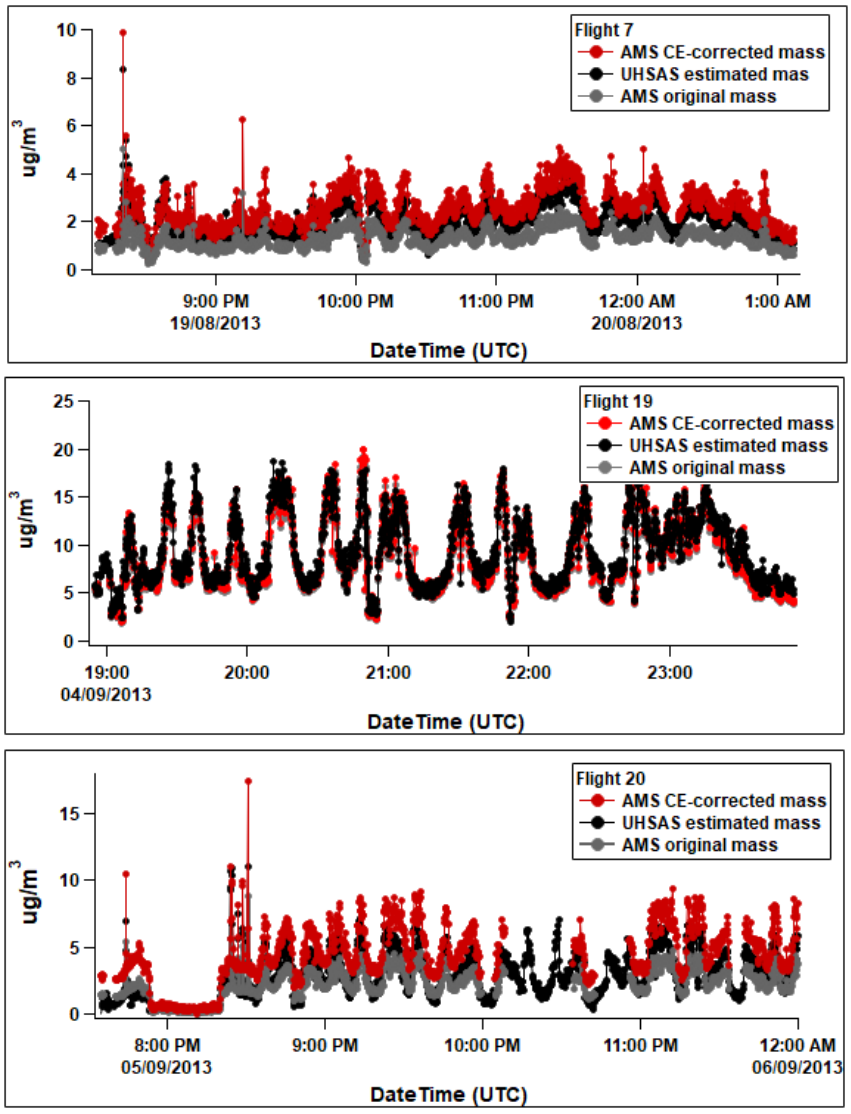

Figure S1. AMS total mass (Σ(p-Organics, pSO_4, pNO_3, pNH_4)) (gray points) compared with mass estimated from the UHSAS (black points) and the AMS CE-corrected mass (red points). The particle collection efficiency (CE) of the AMS was investigated by comparing the total AMS-derived mass with the mass estimated from the size distribution measurements of the UHSAS. Number concentrations measured by the UHSAS over a size range of 60 nm to 1µm (matching that of the AMS) were converted to volume concentrations using mid-point bin diameters and assuming spherical shapes. Volume concentrations were then converted to mass concentrations using densities weighted by the AMS components. A CE of 0.5 was determined for both F7 and F20, and for F19 it was 1.0. Detailed investigations and discussions on the CE of the AMS can be found in the literature (e.g. Middlebrook et al., 2012; Dunlea et al., 2009; Kleinman et al., 2008; Quinn et al, 2006).

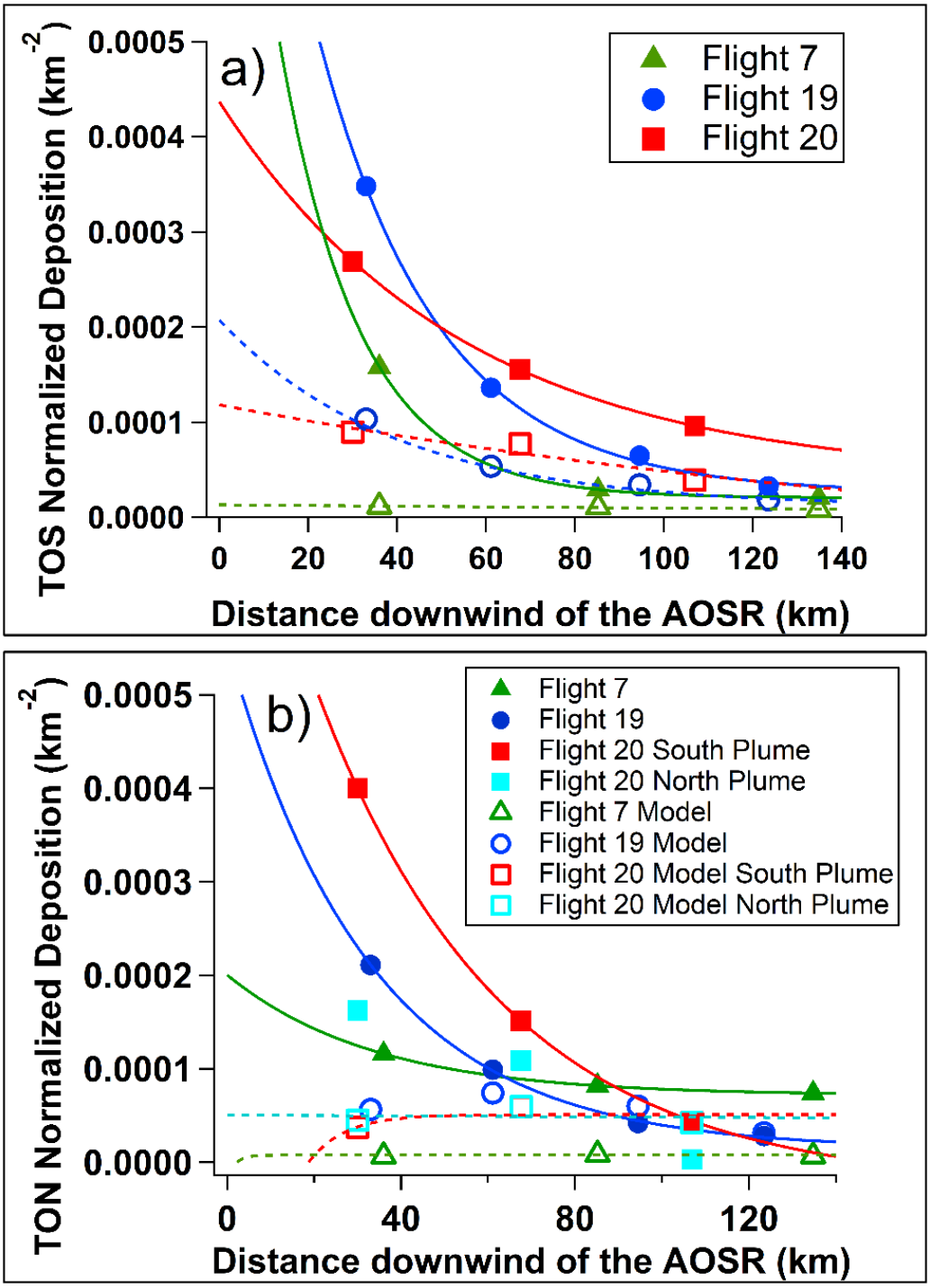

Figure S2. Emissions-normalized deposition fluxes of (a) **TOS** and (b) **TON** derived from the aircraft-based measurements (solid symbols and lines) and the GEM-MACH model (open symbols and dashed lines).

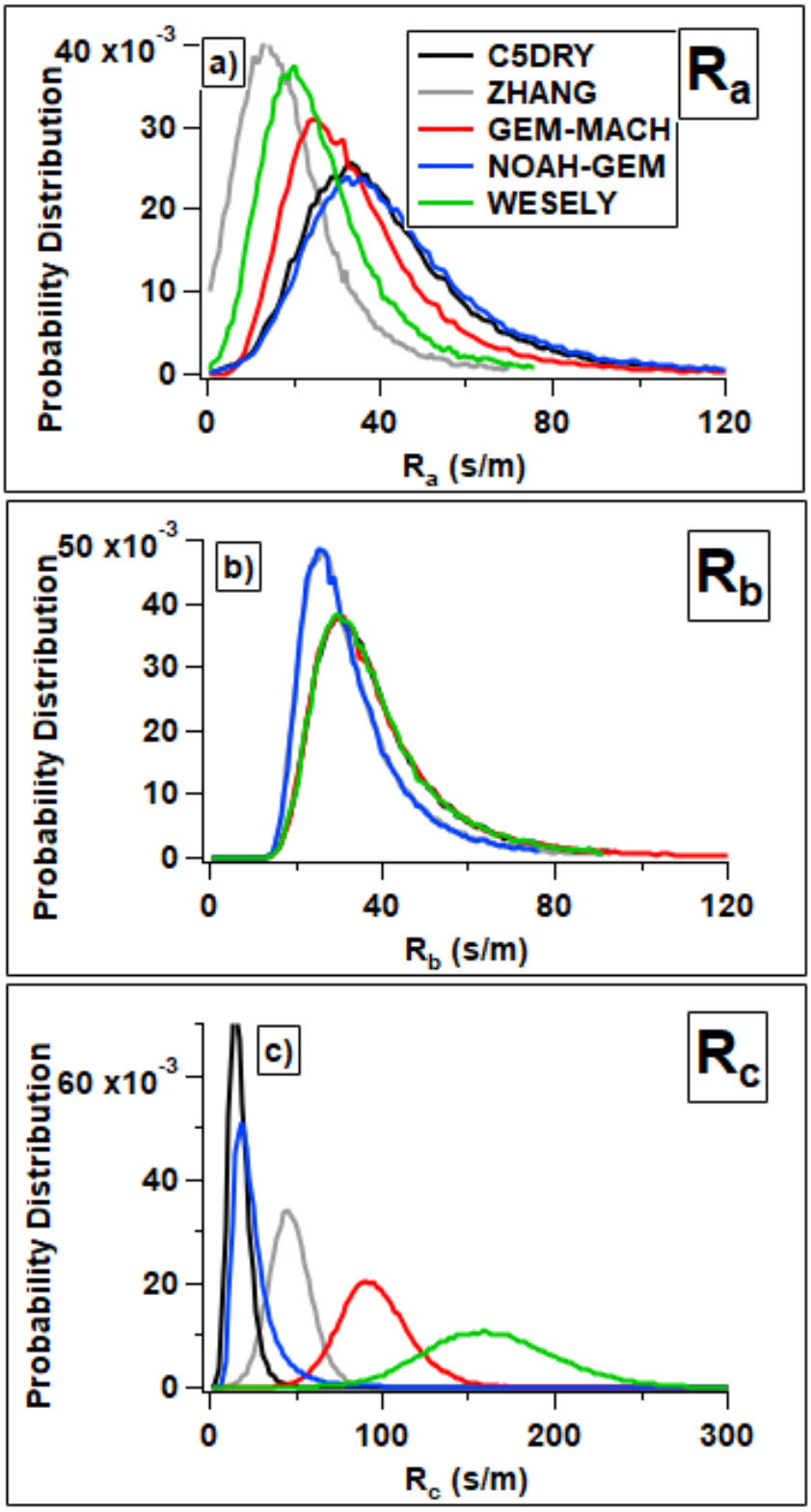

Figure S3. Probability distributions of a) R_a, b) R_b, and c) R_c (s/m) for SO_2 derived from Monte Carlo simulations using 5 different deposition algorithms.

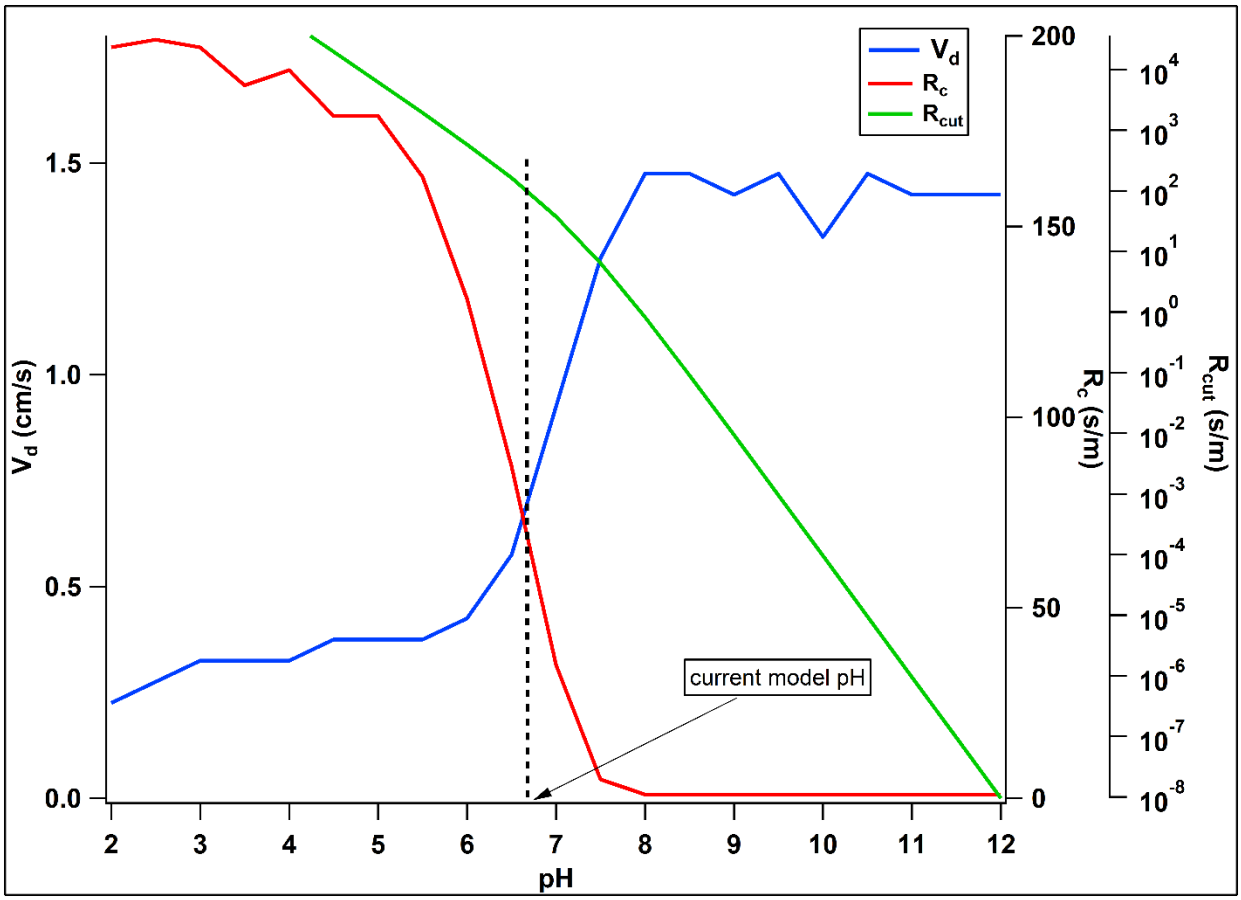

Figure S4 R_{cut}, R_c, (s/m) and V_d (cm/s) for SO_2 as a function of pH as derived from Monte Carlo simulations with the GEM-MACH deposition algorithm.

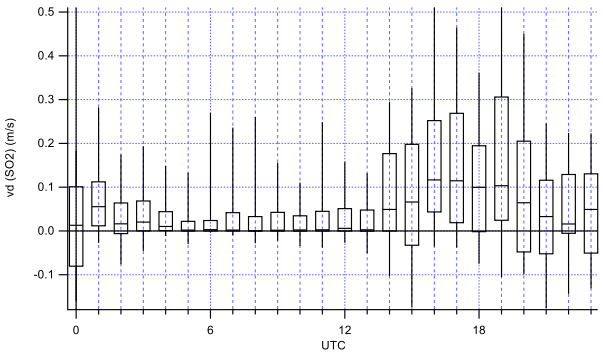

Figure S5. A strong diurnal cycle was seen in the V_d for SO_2 as determined from the vertical gradient methodology at the Oski-ôtin site in the AOSR, with a full stability correction (S24). Essentially no uptake of SO_2 was found during the night. Such a diurnal cycle in the V_d mirrors the diurnal cycle of eddy diffusivity observed at this site.

Section S3. Ground-based SO_2 fluxes. SO_2 fluxes were estimated using an eddy covariance/vertical gradient method with data collected on a 32m tower at the Oski-ôtin air quality station (57.1837 ^{o} N, 111.6395 ^{o} W) in Fort McKay, centrally located in the AOSR. The observation method was similar to that reported previously (Wu et al., 2018); ultrasonic anemometers (model CSAT-3, Campbell Scientific, USA) were collocated with inlets of ½" Teflon tubing at 32m, 18m and 8m above ground, drawing sampled air to gas analyzers at the base of the tower (Thermo Environmental 43i TCL). Data presented here were collected between June 6-8, 2018. Eddy diffusivities were calculated from the difference in wind speed at 32m and 8m combined with the momentum flux determined through eddy covariance at 18m, and stability-corrected following Högström et al. 1996. The determined dry deposition velocities for SO_2 are shown in Figure S4. Only daytime data (between 19 and 1 UTC) unaffected by structural disturbances (e.g. flow through the tower) were included in the comparison with the aircraft results aligning with the typical flight times. Resulting deposition velocities for SO_2 had a median of 4.1 cm s^{-1} and a trimmed mean of 4.9 cm s^{-1} (standard error 1.2 cm s^{-1}).

Section S4. SO_2 chemical losses

The most significant oxidant that reacts in the gas phase with SO_2 is the hydroxyl radical, OH, to produce H_2SO_4. Previous aircraft studies have shown that, in the absence of clouds, SO_2 oxidation by OH is the main pathway for SO_2 loss in industrial plumes in summertime (Brock et al., 2002; Miyakawa et al., 2007). The transformation flights were all conducted during midday under clear sky conditions, hence the contribution of cloud aqueous chemistry towards pSO_4 production during the study flights is minimal. The potential loss of SO_2 to reactions with alkenes to form organosulfates (Shang et al., 2016) and with criegee biradicals to form H_2SO_4 (Boy et al., 2013; Mauldin et al, 2012; Huang et al., 2015) would not be accounted for in the mass balance of the S mass in SO_2 presented above but would be <1% of the SO_2 conversion. Regardless, since sulfates are detected as pSO_4 by the AMS (Farmer et al., 2010), any SO_2 chemical loss other than by the reaction with OH would still be captured in the mass balance of **TOS**.

OH concentrations were estimated using ratios of selected volatile organic compounds (VOCs) that react almost exclusively with OH (during the daytime) and a methodology as described previously (Kleinman et al., 2003). Lagrangian transport times were determined from the aircraft-based wind speed measurements and the transit time of air between successive screens (Liggio et al., 2016). It is possible that there will be cross plume gradients in SO_2 and VOC concentrations given their different sources from each facility. However, the VOC canisters were not instantaneous, but were ~ 30 s long, representing a spatial grab of ~ 2-3 km at the speed of the aircraft. These VOC's represent the average VOC concentration from numerous sources on site, and their spatial footprint overlaps significantly with the SO_2 source footprint in these facilities. The uncertainties ranged from 17 to 58%, which attempts to account for uncertainties associated with the selection of the reference hydrocarbon concentrations, the slope determination, transport times, and reaction rate constants. OH concentrations derived using the ratio of toluene to benzene and plume box modeling for F19 (Liggio et al., 2016) were consistent within the uncertainties.

Section S5. Modelled dry deposition fluxes and dry deposition velocities

Dry deposition fluxes estimated are compared with those predicted from an air quality model, Global Environmental Multiscale – Modelling Air-quality and CHemistry (GEM-MACH). GEM-MACH is a comprehensive on-line chemical reaction transport model (Moran et al., 2010) that has recently been used to estimate acidic deposition downwind of the AOSR (Makar et al., 2018) using a 2.5 km grid cell resolution. A detailed description of GEM-MACH appears elsewhere (Makar et al., 2018; Akingunola et al., 2018; Gordon et al., 2018). The model includes parameterizations for gas-phase chemistry, aqueous chemistry and cloud processing of gases and aerosols, inorganic heterogeneous chemistry, secondary organic aerosol formation, and aerosol microphysics. The model version used here employs a 12-bin sectional approach to resolve particle size distribution, and eight aerosol species (sulfate, nitrate, ammonium, secondary organic aerosol, primary organic aerosol, black carbon, sea-salt, and crustal material), and incorporates aerosol direct and indirect feedbacks with the meteorological code's radiative transfer (Makar et al., 2015a; Makar et al., 2015b). Gas phase deposition of N and S compounds is determined through a commonly used resistance methodology with deposition velocities calculated using inferential methods (Makar et al., 2018). The deposition fluxes are incorporated into the vertical diffusion operator as a flux boundary condition. Further details on the formulation of GEM-MACH are provided elsewhere (Makar et al., 2018 and references therein).

The model plume boundaries were determined separately for NO_x and SO_2 plumes, using the assumption that the plume edge corresponds to background concentrations, as was the case for the observed plumes. Model and observed screens did not necessarily spatially coincide due to differences between the modelled and observed wind fields (Tables 1, 2). However, the same strategy was used to set up downwind model screen locations as in the observations (specifically, determining the plume center at one hour's advection time downwind from the sources, placing the first screen perpendicular to this direction and centred on the plume centreline, calculating a one-hour forward trajectory for the second screen and repeating the process for the second and subsequent screens). The intersection of the screen lines with the 0.1 maximum concentration contours for SO_2 and NO_x respectively, determined the boundaries of the screens for the SO_2 and NO_x plumes. Boundaries were also adjusted to correspond with the 0.2 and 0.3 maximum concentration contours which resulted in small differences (<5%) in the derived deposition fluxes. In F7, the modelled and actual plume locations were very similar; however, in F19 and F20, the modelled plumes were not exactly in the same geographical location as the observations because of differences in advection direction (Tables 1, 2).

The spatially averaged dry deposition velocities for SO_2, pSO_4 and TON are compared with those obtained using inferential methods from GEM-MACH. The measurement and model results for all three flights are listed in Table S2.

Section S6. References

Akingunola, A., Makar, P.A., Zhang, J., Darlington, A., Li, S.-M., Gordon, M., Moran, M.D. and Zheng, Q.: A chemical transport model study of plume-rise and particle size distribution for the Athabasca oil sands, Atmos. Chem. Phys., **18**, 8667-8688, 2018.

Baldocchi, D.D., Vogel, C.A. and Hall, B.: Seasonal variation of carbon dioxide exchange rates above and below a boreal jack pine forest, Agri, and Forest Meteor., **83**, 147-170, https://doi.org/10.1016/S0168-1923(96)02335-0, 1997.

Boy, M., Mogensen, D., Smolander, S., Zhou, L., Nieminen, T., Paasonen, P., Plass-DÜlmer, C., Sipilä, M., Petäjä, T., Mauldin, L., Berresheim, H. and Kulmala, M.: Oxidation of SO_2 by stabilized criegee intermediate (sCI) radials as a crucial source for atmospheric sulfuric acid concentrations, Atmos. Chem. Phys., **13**, 3865-3879, doi:10.5194/acp-13-3865-2013, 2013.

Brock, C.A., Washenfelder, R.A., Trainer, M., Ryerson, T.B., Wilson, J.C., Reeves, J.M., Huey, L.G., Holloway, J.S., Parrish, D.D., Hübler, G., Fehsenfeld, F.C.:, J. Geophys. Res. **107** (D12), 4155, 2002.

Brook, J.R., Zhang, L., Di-Giovanni, F. and Padro, J.: Description and evaluation of a model of deposition velocities for routine estimates of air pollutant dry deposition over North America. Part I: model development, Atmos. Environ., **33**, 5037-5051, https://ui.adsabs.harvard.edu/link_gateway/1999AtmEn..33.5053B/doi:10.1016/S1352-2310(99)00251-4, 1999.

Dunlea, E.J., DeCarlo, P.F., Aiken, A.C., Kimmel, J.R., Peltier, R.E., Weber, R.J., Tomlinson, J., Collins, D.R., Shinozuka, Y., McNaughton, C.S., Howell, S.G., Clarke, A.D., Emmons, L.K., Apel, E.C., Pfister, G.G., van Donkelaar, A., Martin, R.V., Millet, D.B., Heald, C.L., Jimenez, J.L., Evolution of Asian aerosols during transpacific transport in INTEX-B, Atmos. Chem. Phys., 9, 7257-7287, https://doi.org/10.5194/acp-9-7257-2009, 2009.

Farmer, D.K., Matsunaga, A., Docherty, K.S., Surratt, J.D., Seinfeld, J.H., Ziemann, P.J. and Jimenez, J.L.: Response of an aerosol mass spectrometer to organonitrates and organosulfates and implications for atmospheric chemistry, PNAS, **107**, 6670-6675, https://doi.org/10.1073/pnas.0912340107, 2010.

Gordon, M., Makar, P.A., Staebler, R.M., Zhang, J., Akingunola, A., Gong, W. and Li, S.-M.: A comparison of plume rise algorithms to stack plume measurements in the Athabasca oil sands, Atmos. Phys. Chem., **18**, 14695-14714, https://doi.org/10.5194/acp-18-14695-2018, 2018.

Grassi, S., Junghans, S. and Raubal, M.: Estimating mean annual energy production of clustered wind turbines with GIS, Intern. Conf. on Appl. Energy, Paper ID: ICAE2013-492, 2013.

Högström, U.: Review of some basic characteristics of the atmospheric surface layer, Boundary-Layer Meteo., **78**, 215-246, doi:10.1007/bf00120937, 1996.

Huang, H.-L., Chao, W. and Jr-Min Lin, J.: Kinetics of a criegee intermediate that would survive high humidity and may oxidize atmospheric SO_2, PNAS, **112 (35)**, 10857-10862, https://doi.org/10.1073/pnas.1513149112, 2015.

Kleinman, L.I., Daum, P.H., Lee, Y.-N., Nunneermacker, L.J., Springston, S.R., Weinstein-Lloyd, J., Hyde, P., Doskey, P., Rudolph, J., Fast, J. and Berkowitz, C.: Photochemical age determinations in the Phoenix metropolitan area, *J. Geophys. Res.*, **108 (D3)**, 4096, https://doi.org/10.1029/2002JD002621, 2003.

Kleinman, L.I., Springston, S.R., Daum, P.H., Lee, Y.-N., Nunnermacker, L.J., Senum, G.I., Wang, J., Weinstein-Lloyd, J., Alexander, M.L., Hubbe, J., Ortega, J., Canagaratna, M.R., and Jayne, J., The time evolution of aerosol composition over the Mexico City plateau, Atmos. Chem. Phys., 8, 1559-1575, https://doi.org/10.5194/acp-8-1559-2008, 2008.

Liggio, J., Li, S.-M., Hayden, K., Taha, Y. M., Stroud, C., Darlington, A., Drollette, B.D., Gordon, M., Lee, P., Liu, P., Leithead, A., Moussa, S.G., Wang, D., O'Brien, J., Mittermeier, R.L., Brook, J.R., Lu, G., Staebler, R.M., Han, Y., Tokarek, T.W., Osthoff, H.D., Makar, P.A., Zhang, J., Plata, D.L., Gentner, D.R.: Oil sands operations as a large source of secondary organic aerosols, Nature, **534**, 91, https://doi.org/10.1038/nature17646, 2016.

Makar, P.A., Gong, W., Milbrandt, J., Hogrefe, C., Zhang, Y., Curci, G., Zabkar, R., Im, U., Balzarini, A., Baró, R., Bianconi, R., Cheung, P., Forkel, R., Gravel, S., Hirtl, M., Honzak, L., Hou, A., Jiménez-Guerrero, P., Langer, M., Moran, M.D., Pabla, B., Pérez, J.L., Pirovano, G., San José, R., Tuccella, P., Werhahn, J., Zhang, J. and Galmarini, S.: Feedbacks between air pollution and weather, Part 1: Effects on weather, Atmos. Environ., **115**, 442-469, https://doi.org/10.1016/j.atmosenv.2014.12.003, 2015a.

Makar, P.A., Gong, W., Hogrefe, C., Zhang, Y., Curci, G., Zabkar, R., Milbrandt, J., Im, U., Balzarini, A., Baró, R., Bianconi, R., Cheung, P., Forkel, R., Gravel, S., Hirtl, M., Honzak, L., Hou, A., Jiménez-Guerrero, P., Langer, J., Moran, M.D., Pabla, B., Pérez, J.L., Pirovano, G., San José, R., Tuccella, P., Werhahn, J., Zhang, J. and Galmarini, S.: Feedbacks between air pollution and weather, Part 2: Effects on chemistry, Atmos. Environ., **115**, 499-526, https://doi.org/10.1016/j.atmosenv.2014.10.021, 2015b.

Makar, P.A., Staebler, R.M., Akingunola, A., Zhang, J., McLinden, C., Kharol, S.K., Pabla, B., Cheung, P. and Zheng, Q.: The effects of forest canopy shading and turbulence on boundary layer ozone, Nature Com., **8**, 15243, https://doi.org/10.1038/ncomms15243, 2017.

Makar, P.A., Akingunola, A., Aherne, J., Cole, A.S., Aklilu, Y., Zhang, J., Wong, I., Hayden, K., Li, S.-M., Kirk, J., Scott, K., Moran, M.D., Robichaud, A., Cathcart, H., Baratzedah, P., Pabla, B., Cheung, P., Zheng, Q. and Jeffries, D.S.: Estimates of exceedances of critical loads for acidifying deposition in Alberta and Saskatchewan, Atmos. Chem. Phys., **18**, 9897-9927, https://doi.org/10.5194/acp-18-9897-2018, 2018.

Massman, W.J.: A review of the molecular diffusivities of H_2O, CO_2, CH_4, CO, O_3, SO_2, NH_3, N2O, NO, and NO_2 in air, O_2 and N_2 near STP, *Atmos. Environ*., **32 (6)**, 1111-1127, https://doi.org/10.1016/s1352-2310(97)00391-9, 1998.

Mauldin III, R.L., Berndt, T., Sipilä, M., Paasonen, P., Petäjä, T., Kim, S., Kurté, T., Stratmann, F., Kerminen, V.-M. and Kulmala, M.: A new atmospherically relevant oxidant of sulphur dioxide, Nature, **488**, 193-197, https://doi.org/10.1038/nature11278, 2012.

Middlebrook, A.M., Bahreini, R., Jimenez, J.L., and Canagaratna, M.R., Evaluation of composition-dependent collection efficiencies for the Aerodyne Aerosol Mass Spectrometer using field data, Aerosol. Sci. Technol., 46, 258-271, doi: 10.1080/02786826.2011.620041, 2012.

Miyakawa, T., Takegawa, N. and Kondo Y.: Removal of sulfur dioxide and formation of sulfate aerosol in Tokyo, J. Geophys. Res., **112**, D13209, doi:10.1029/2006JD007896, 2007.

Moran, M.D., Ménard, S., Pavlovic, R., Anselmo, D., Antonopoulos, S., Makar, P.A., Gong, W., Gravel, S., Stroud, C., Zhang, J., Zheng, Q., Robichaud, A., Landry, H., Beaulieu, P.A., Gilbert, S., Chen, J. and Kallaur, A.: Recent Advances in Canada's national operational AQ forecasting system, In: Steyn DG, Rao ST (Eds) Air Pollution Modelling and Its Application, Springer, Dordrecht, 289, 2010.

Niyogi, D., Alapaty, K., Raman, S. and Chen, F.: Development and evaluation of a coupled photosynthesis-based gas exchange evapotranspiration model (GEM) for mesoscale weather forecasting applications, J. Appl. Meteor. and Climatol., **48**, 349-368, https://doi.org/10.1175/2008JAMC1662.1, 2009.

Quinn, P.K., Bates, T.S., Coffman, D., Onasch, T.B., Worsnop, D., Baynard, T., de Gouw, J.A., Goldan, P.D., Kuster, W.C., Williams, E., Roberts, J.M., Lerner, B., Stohl, A., Pettersson, A., and Lovejoy, E.R., Impacts of sources and aging on submicrometer aerosol properties in the marine boundary layer across the Gulf of Maine, J. Geophys. Res., 111, D23S36, doi.10.1029/2006JD007582, 2006.

Shang, J., Passanantis, M., Dupart, Y., Ciurarus, R., Tinel, L., Rossignol, S., Perrier, S., Zhu, T. and George, C.: SO_2 uptake on oleic acid : a new formation pathway of organosulfur compounds in the atmosphere, Environ. Sci. Technol. Lett. **3**, 67-72, https://doi.org/10.1021/acs.estlett.6b00006, 2016.

Wesley, M.L.: Parameterization of surface resistances to gaseous dry deposition in regional-scale numerical models, Atmos. Environ., **23**, 1293-1304, https://ui.adsabs.harvard.edu/link_gateway/1989AtmEn..23.1293W/doi:10.1016/0004-6981(89)90153-4, 1989.

Wu, Z. Schwede, D.B., Vet, R., Walker, J.T., Shaw, M., Staebler, R. and Zhang, L.: Evaluation and intercomparison of five North American dry deposition algorithms at a mixed forest site, J. Adv. Modelling Earth Systems, **10,** 1571-1586, , 2018.Zhang, L., Brook, J.R. and Vet, R.: A revised parameterization for gaseous dry deposition in air-

quality models, Atmos. Chem. Phys. **3**, 2067-2082, https://doi.org/10.5194/acp-3-2067-2003, 2003.

Zhang, L., Moran, M.D., Makar, P.A., Brook, J.R. and Gong, S.: Modelling gaseous dry deposition in AURAMS: a unified regional air-quality modelling system, Atmos. Environ., **36**, 537-560, https://doi.org/10.1016/S1352-2310(01)00447-2, 2002.